Chemistry–A European Journal

Research Article
doi.org/10.1002/chem.202500474

Chemistry Europe
European Chemical Societies Publishing

www.chemeurj.org

Differentiating Ligand Tailoring and Cation Incorporation as Strategies for Tuning Heterobimetallic Cerium Complexes

Emily R. Mikeska[a, b] and James D. Blakemore*[a]

Tuning of redox-active complexes featuring metals with high coordination numbers by incorporation of secondary redox-inactive cations has received far less attention than it deserves. Here, appending moderate steric bulk to a tripodal ligand framework has been tested for its influence on secondary-cation-driven structural and electrochemical tuning of cerium, a lanthanide that tends to adopt high coordination numbers. A *quasi*-C_3-symmetric cerium(III) complex denoted **[Ce]** has been prepared that features pendant benzyloxy groups, and this work demonstrates that this species offers a site capable of binding single Na^+ or Ca^{2+} ions. Electrochemical and UV-visible spectroscopic studies reveal equilibrium binding affinity of **[Ce]** for Na^+ in acetonitrile solvent, contrasting with tight binding of all cations in all other previously studied systems of this type. The modulated cation binding can be attributed to the bulky benzyloxy groups, which impact the thermodynamics of cation binding but do not impede the formation of cerium centers with coordination number 8 upon binding of either Na^+ or Ca^{2+}. The Ce(IV/III) reduction potential was found to be tunable under the equilibrium binding conditions, highlighting the potentially significant role that controlled structural changes can play in modulating the solution properties of heterobimetallic complexes.

1. Introduction

While the lanthanide elements are conventionally found in their +III oxidation states, others are accessible as well. The +II oxidation state (O.S.) has been demonstrated to be accessible across the series, and the +IV state is known for molecular complexes of praseodymium, terbium, and cerium.[1–6] However, cerium is the lanthanide that is most well known to be redox active; the accessibility of both +III and +IV complexes gives rise to useful chemical properties, and these have encouraged applications in homogeneous and heterogeneous catalysis.[7,8] Accessing particular oxidation states for the lanthanides relies, in part, on selection of appropriate ligand systems, highlighting the role of ligand-promoted control over the properties of cerium centers. For example, use of multiple anionic donor ligands has been shown to shift the Ce(IV/III) reduction potential to more negative values in comparison to systems with fewer anionic donors.[9] However, apart from controlling the ligand field, there are few reliable strategies for rationally tuning the reduction potential(s) required to access particular lanthanide oxidation states. This is reflected, in part, in the rather potent reductants required to access molecular complexes containing +II O.S. lanthanides[1,2] and the exotic, strong-field ligands required to access molecular complexes of +IV O.S. lanthanides.[3,4]

Contrasting with the limited control that can currently be exercised over lanthanide reduction potentials, there are several proven strategies for rational tuning of transition metal and actinide reduction potentials. Incorporation of secondary redox-inactive metal cations into otherwise monometallic species has emerged as an effective strategy for the rational (that is to say, uniformly achievable by design) tuning of the properties of redox-active metals. This phenomenon was revealed, in part, through decades of investigation surrounding the role of Ca^{2+} in the Oxygen Evolving Complex (OEC) of Photosystem II, which is itself a heterometallic system of redox-active manganese centers and a redox-inactive Ca^{2+} ion.[10] Studies of metallocubanes as OEC models, as developed by Agapie and co-workers, demonstrated that the redox chemistry of the manganese centers could be tuned by more than a volt when the Ca^{2+} ion was exchanged for other cations (denoted, in general, as **M**), and that this tuning effect was correlated with the effective Lewis acidity of the incorporated redox-active cations.[11] From a fundamental perspective, correlations with Lewis acidity are reasonable when considered as charge density effects, dependent both on a cation's charge and size. Wulfsberg has discussed this charge density concept in detail.[12]

One intuitive, reliable, and broadly useful parametrization of such charge density effects relies on the descriptor used first, to the best of our knowledge, by Agapie and co-workers in examining the redox properties of manganese-containing metallocubanes: the pK_a values of metal aqua complexes, $[\mathbf{M}(H_2O)_m]^{n+}$.[11] While other descriptors for cation-driven tunability have been investigated, the pK_a values have proven to be the most broadly utilized, likely due in part to the large number of cations for which experimental pK_a values have been measured,

[a] E. R. Mikeska, J. D. Blakemore
Department of Chemistry, University of Kansas, 1567 Irving Hill Road, Lawrence, Kansas 66045, USA
E-mail: blakemore@ku.edu

[b] E. R. Mikeska
Chemical Sciences and Engineering Division, Argonne National Laboratory, Lemont, Illinois 60439, USA

Supporting information for this article is available on the WWW under https://doi.org/10.1002/chem.202500474

as tabulated in Perrin's well-known and useful catalogue.[13] Along the same line, Greb and co-workers have focused on quantifying the Lewis acidity of neutral and charged species, as well as differentiating between the global, effective, and intrinsic Lewis acidity of such compounds.[14] Despite the complexities of quantifying and comparing Lewis acidities of various compounds, there is a coincidental co-linear correlation between acidity in acetonitrile and water; consequently, the scale measured in water can be concluded to be at least conceptually and at most quantitatively applicable in acetonitrile.[15] Acetonitrile, of course, is among the most common solvents for studies of nonaqueous redox chemistry, further amplifying the value of the (aqueous) pK_a scale.

On this theme, the effects of secondary metal cations on the electrochemical, spectroscopic, and structural properties of multimetallic complexes have been extensively explored.[16] The first work from our group in this arena examined heterobimetallic complexes of nickel and redox-inactive cations Na^+, Ca^{2+}, Nd^{3+}, and Y^{3+}; this study was notable in expanding quantitative analyses of tuning to trivalent lanthanides. The redox chemistry of the nickel complexes was rationally tuned by the incorporation of the cations, inducing a shift in the peak cathodic reduction potential ($E_{p,c}$) for $Ni^{II/I}$ redox by 70 ± 12 mV/pK_a unit.[17] Subsequent investigations by our group have probed tuning in complexes of uranyl,[18,19] zinc,[20] nickel,[21] palladium,[22] and vanadyl.[23] These studies have revealed reliable, monotonic, and structurally sensitive relationships between the Lewis acidity (pK_a) of incorporated cations and electrochemical reduction potential(s), demonstrating the broad appeal of secondary cation–driven tuning.

Turning to lanthanide chemistry, however, we would foreground the high variability of metal coordination number and geometry as challenges faced when attempting to gain control over lanthanide properties such as reduction potentials. One set of complexes developed by Schelter and co-workers, supported by a BINOLate-type ligand framework, served as a model system to test cation-driven effects on cerium (see Figure 1).[24–26] In this system, Ce(IV/III) reduction potentials for 1:3 Ce:**M** complexes with alkali cations (**M** = Li^+, Na^+, K^+, and Cs^+) spanned a range of 450 mV, a substantial effect requiring three secondary cations that was not found to depend on Lewis acidity. Benefits of the BINOLate ligand include its ability to lower the coordination number of cerium to 6 or 7 and to facilitate controlled assembly of 1:3 Ce:**M** complexes. However, the coordination numbers of cerium are decreased from those displayed by less artificially constrained species (for example, $[Ce(H_2O)_9]^{3+}$). In an alternative approach to heterometallic complexes that did not address redox chemistry, Costes and co-workers pioneered an application of Orvig's trensal-type ligands for the capture of two high coordination number lanthanides for studies of magnetism (Figure 1).[27,28] More recently, La Pierre and co-workers investigated a series of tetrahedral cerium complexes where, despite being constrained to a low coordination number, tuning of the structural, redox, and electronic properties of the cerium center was achieved based on the identities of incorporated alkali metal cations.[29]

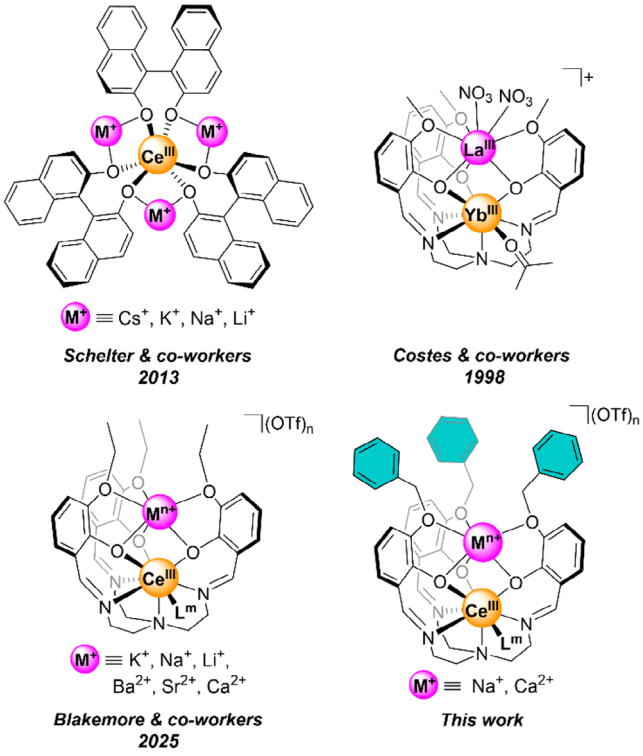

Figure 1. Selected examples of heterobimetallic complexes of lanthanide(III) ions relevant to this work. Benzyl groups are highlighted to show increased steric bulk compared to Blakemore and co-workers, 2025.[30]

Our group has extended investigations of cation-driven tuning of cerium to heterobimetallic complexes with mono- and divalent cations[30] to explore tuning effects in complexes that allow cerium to retain its natural bonding preference for high coordination numbers (see Figure 1).[31–41] Through the use of a trensal-inspired tripodal ligand framework featuring a heptadentate [N_4,O_3] binding site for cerium and a hexadentate site for secondary cation binding, stereochemical control at the cerium centers could be maintained across bimetallic complexes of Ce with both monovalent and divalent metal ions displaying a range of Lewis acidities. The largest electrochemical tuning range achieved to date for 1:1 heterobimetallic complexes of more than 600 mV was measured for the family of compounds and could be described by a linear relationship between the pK_a of the cations and the reduction potential, underscoring the ability to rationally tune lanthanide redox in this system. However, the multi-compartment nature of the tripodal ligand system used in this work suggested to us that an opportunity to better deconvolute cation- and ligand-driven effects might lie in derivatization of the cation-binding site. We envisioned that such an effort could afford insights into the interplay between cation identity, ligand structure, and the chemical properties achievable in the solution phase.

Here, we report the synthesis and characterization of a set of cerium(III) compounds assembled with a tailored ligand that is suitable for co-encapsulation of cerium and secondary metal cations. The properties of a nascent hexadentate site, oriented for secondary cation binding in close proximity (≤3.6 Å) to

cerium, were purposefully modulated in the ligand system by incorporation of benzyloxy groups; these groups were chosen in order to probe the effect of a small, controlled structural change on the overall properties and electrochemical tuning behavior of the complexes upon incorporation of either Na^+ or Ca^{2+} as secondary cations. X-ray diffraction (XRD) analysis of the monometallic cerium complex, as well as the bimetallic complexes of Na^+ and Ca^{2+}, revealed that a structurally motivated model could be used to interpret solution properties and compare the benzyloxy-substituted complexes to prior ethoxy-substituted species. The binding affinity of the hexadentate cavity for Lewis acids was investigated with spectrochemical titrations, indicating that incorporation of the benzyloxy groups leads to equilibrium binding of less acidic Na^+ but affords tight binding of more acidic Ca^{2+}. The Ce(IV/III) potential was tuned by 630 mV upon incorporation of Ca^{2+}, while the diminished affinity of the hexadentate site for Na^+ resulted in a measurable perturbation of the otherwise anticipated cation-driven potential shift, confirming the centrality of ligand-cation host-guest thermodynamic preferences in promoting redox tunability. Taken together, the findings reported here add to the growing inventory of established characteristics that can be encountered in cation-driven tuning, particularly for the extremely rarely studied case of high coordination number lanthanide (or actinide) centers.

2. Results

2.1. Synthesis and Characterization of Monometallic and Heterobimetallic Complexes of Ce^{3+}

The original trensal-type ligands were not capable of incorporating additional metal centers under the chosen synthetic conditions,[27,36–38] but subsequent iterations incorporated methoxy substituents (and others)[39] on the aromatic rings of the ligand to enable the housing of two metals, as in heterobimetallic complexes.[34] Several other reports have since presented additional lanthanide complexes of this methoxy-substituted tripodal ligand which focus on the solid-state magnetic properties; little solution-phase characterization is available as the methoxy-substituted complexes are soluble in methanol but insoluble in aprotic solvents (such as acetonitrile and dichloromethane) suitable for interrogation of redox and other properties under air- and water-free conditions.[40–44] A recent report by our group built upon this wealth of prior work and moved to an ethoxy-substituted tripodal ligand denoted H_3L^{OEt} which increased the solubility in aprotic solvents suitable for solution-phase inert atmosphere studies and enabled rich solution-phase characterization.[30] (Two lanthanide complexes of the ethoxy-substituted tripodal ligand had been reported prior to our work, but only structural data are available for those complexes.[45])

Here, a benzyloxy-substituted ligand derivative (tris(((2-hydroxy-3-benzyloxybenzyl)amino)ethyl) amine), denoted H_3L^{OBn} (shown in Scheme 1), was prepared which maintains

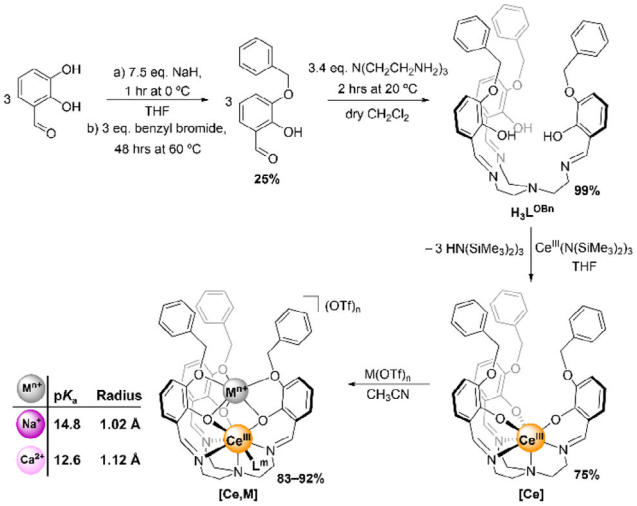

Scheme 1. Synthetic pathway to access H_3L^{OBn}, **[Ce]**, and heterobimetallic complexes **[Ce,Na]** and **[Ce,Ca]**.

the same "lower" heptadentate site of H_3L^{OEt} but contains benzyloxy substituents at the *ortho* positions of the three phenyl rings that link the "upper" and "lower" cavities. With these groups in place, an upper hexadentate cavity could be formed upon cerium binding, similar to the case explored in our prior work.[30] In addition to preserving the desired solubility properties, we made this targeted change to the upper hexadentate cavity by way of benzyloxy substituents to probe the orthogonal effects of ligand modification versus Lewis acid incorporation, while maintaining the ability to directly compare structural changes, binding capabilities, and electrochemical properties with the ethoxy-substituted complexes of our group's prior study (denoted hereafter as $[Ce]^{OEt}$ or $[Ce,M]^{OEt}$; see *Blakemore and co-workers 2025* in Figure 1).[30]

Regarding the comparison of the benzyloxy ligand H_3L^{OBn} reported here and the prior H_3L^{OEt}, it should probably be noted that the terminal phenyl and methyl groups (associated with the benzyl and ethyl substituents, respectively), in these two ligand variants differ in a number of ways. Phenyl is planar, features a π-system, and presents unequal steric bulk upon $C_{methylene}$–C_{phenyl} bond rotation. Methyl is tetrahedral, lacks a π-system, and presents equal steric bulk upon $C_{methylene}$–C_{methyl} rotation. As a reviewer suggested, comparison of neopentyloxy and ethyloxy could have avoided some of these variations. However, despite the multiple points of difference between the H_3L^{OBn} and H_3L^{OEt} systems, the results of our study can, in general, be satisfactorily interpreted on the grounds of steric arguments (rather than necessitating treatment of differences in electronegativity, conjugation, or quadrupole) between the benzyloxy and ethyloxy substituents.

Following installation of the benzyl group onto 2,3-dihydroxybenzaldehyde by a modified literature procedure,[46] H_3L^{OBn} was prepared by imine condensation in dry dichloromethane and its formation was confirmed by ^1H NMR and infrared spectroscopy, as well as high-resolution mass spectrometry (HR-MS). As the reactions to form the ligand give fair results on the gram scale, large quantities of H_3L^{OBn} (ca. 4

g) could be prepared over the course of 3 days. All available data confirmed the successful generation of the desired new ligand $\mathbf{H_3L^{OBn}}$ (see the Experimental Section for details on the modified procedure and Supporting Information, Figures S1, S2, S15, S16, and S18 for spectra). Subsequently, metalation with Ce(III) was accomplished in tetrahydrofuran (THF) by employing tris(bis(trimethylsilyl)amido)cerium(III), a species containing three equivalents of basic hexamethyldisilazane moieties that can serve to deprotonate the phenolic protons of $\mathbf{H_3L^{OBn}}$ and yield the Ce-monometallic complex **[Ce]** as a lustrous orange precipitate (Scheme 1).

In solution, the ^{1}H NMR spectrum of **[Ce]** shows 11 peaks, several of which are paramagnetically shifted. All diamagnetic features associated with $\mathbf{H_3L^{OBn}}$ are absent, indicating successful incorporation of the $4f^1$ Ce^{3+} ion into the ligand (see Supporting Information, Figure S3). The resonance likely associated with the imine protons is particularly affected by the paramagnetic center in **[Ce]** and shifts to 17.57 ppm compared to 14.05 ppm in $\mathbf{H_3L^{OBn}}$. In addition, a feature appears at −8.16 ppm in the spectrum of **[Ce]** (integrating to approximately 6 protons) which likely corresponds to protons of the ethylene backbone of the lower cavity and is significantly shifted due to the close proximity of these protons to the paramagnetic center. Consistent with the weaker effect of paramagnetic centers on more distant NMR-active nuclei, the signals likely associated with the distal aromatic rings of the benzyloxy groups of the upper cavity in **[Ce]** (4.86 ppm (d, 6H), 6.26 ppm (t, 6H), and 6.52 ppm (t, 3H)) remain approximately in the conventional diamagnetic aromatic region of the spectrum and display roofing toward each other (indicative of strong coupling as is often observed for protons associated with each other in the same aromatic ring). The signals likely associated with the proximal phenyl rings of **[Ce]** (those in the chelating ligand backbone "arms") appear shifted slightly downfield (7.88 ppm (t, 3H), 8.11 ppm (d, 3H), 10.66 ppm (d, 3H)). Finally, the number of peaks, integrated peak ratios, and sum of the integrated peaks are consistent with effective C_3 symmetry of **[Ce]** in solution. This finding suggested to us that the benzyloxy groups would be mutually oriented "upward" for secondary cation binding in **[Ce]**, as shown schematically in Scheme 1.

Heterobimetallic complexes of sodium and calcium could be prepared in a clean fashion in acetonitrile by the addition of the relevant metal triflate salt, $\mathbf{M}^{n+}(OTf^-)_n$, to **[Ce]** in a slightly sub-stoichiometric ratio, giving rise to 1:1 bimetallic complexes (denoted **[Ce,Na]** and **[Ce,Ca]**) in high yields (Scheme 1; see Experimental Section for details). ^{1}H NMR spectra of these compounds show peaks that are shifted and distinct from those associated with **[Ce]**, though effective C_3 symmetry is still evident from the number of features present (see Supporting Information, Figures S5 and S8). Notably, the signals in **[Ce,Na]** are significantly broadened compared to both **[Ce]** and **[Ce,Ca]**, possibly a result of an in–out equilibrium of Na^+ in the upper, hexadentate cavity; this broadness is absent from the spectrum of **[Ce,Ca]**, suggesting tight binding likely due to the more Lewis acidic nature of Ca^{2+} (see Supporting Information, Figure S11). The imine resonances remain affected by the paramagnetism of the Ce^{3+} center upon secondary cation binding and shift from 17.57 ppm in **[Ce]** to 11.42 ppm in **[Ce,Na]** and 13.97 ppm in **[Ce,Ca]**, while the protons associated with the distal benzyl rings display the expected splitting, roofing effects, and chemical shifts typical of aromatic protons (between 7.18 and 7.66 ppm for **[Ce,Na]** and between 6.20 and 6.82 ppm for **[Ce,Ca]**).

Compared to the spectrum of $\mathbf{[Ce]^{OEt}}$, the NMR signals of **[Ce]** are largely similar in number, shift, and integration ratios, though **[Ce]** prepared in this new work features three additional features corresponding to the aromatic protons of the distal benzyl ring (see Supporting Information, Figure S12). Significant differences become apparent, however, between the spectra of the heterobimetallic complexes of the two families. In particular, the signals associated with the ethylene backbone of the lower cavity are shifted further downfield in the spectrum of **[Ce,Na]** compared to $\mathbf{[Ce,Na]^{OEt}}$ but appear further upfield in the spectrum of **[Ce,Ca]** compared to $\mathbf{[Ce,Ca]^{OEt}}$ (see Supporting Information, Figures S13 and S14). In accord with the observations from NMR that *i*) no diamagnetic impurities were carried along with our desired compounds and *ii*) no scrambling of metal ions between the upper and lower cavities appeared to occur with the compounds, elemental analysis of **[Ce]**, **[Ce,Na]**, and **[Ce,Ca]** confirmed the expected formulations of the compounds and demonstrated the bulk purity of our isolated materials. Although compounds containing Lewis acidic metal cations can sometimes incorporate adventitious water, no water was detected by any of the analysis methods applied to the bulk samples of **[Ce]**, **[Ce,Na]**, or **[Ce,Ca]**.

In solid-state infrared spectra of the synthesized cerium complexes, the imine C═N stretching feature is particularly diagnostic and can be used to interrogate for coordination of cation(s) to the ligand. The C═N stretch shifts from 1628 cm^{-1} in $\mathbf{H_3L^{OBn}}$ to 1618 cm^{-1} in **[Ce]** (see Supporting Information, Figures S18 and S19). Incorporation of Na^+ or Ca^{2+} shifts the C═N stretch of isolated **[Ce,Na]** and **[Ce,Ca]** to 1613 cm^{-1} and 1620 cm^{-1}, respectively, (see Supporting Information, Figures S20 and S21), confirming the binding of the secondary metal cation to **[Ce]**.

2.2. Single Crystal X-Ray Diffraction

Single crystals suitable for X-ray diffraction (XRD) analysis were grown. The resulting structure of **[Ce]** confirmed the incorporation of Ce^{III} into the tripodal ligand $\mathbf{L^{OBn}}$ and revealed a coordination number of 7 for the Ce center, as well as an empty, nascent hexadentate site in the upper portion of the complex poised for the binding of a second metal cation (see Figure 2). Selected bond metrics are provided in Table 1 and crystallographic details are given in the Supporting Information (see Supporting Information, pp. S31–S33). Structures of this type can be described as either Δ or Λ isomers depending on whether the arms of the ligand wrap in a clockwise or counterclockwise fashion, respectively, about the principal axis. **[Ce]** crystallizes in the centrosymmetric space group $P2_1/n$ and the structure displays *quasi*-C_3 symmetry with the Ce-N4 bond approximately co-linear with the principal axis. The centrosymmetric nature of the structure confirms that both the Δ and Λ isomers are present in the solid state in the expected 1:1 ratio anticipated

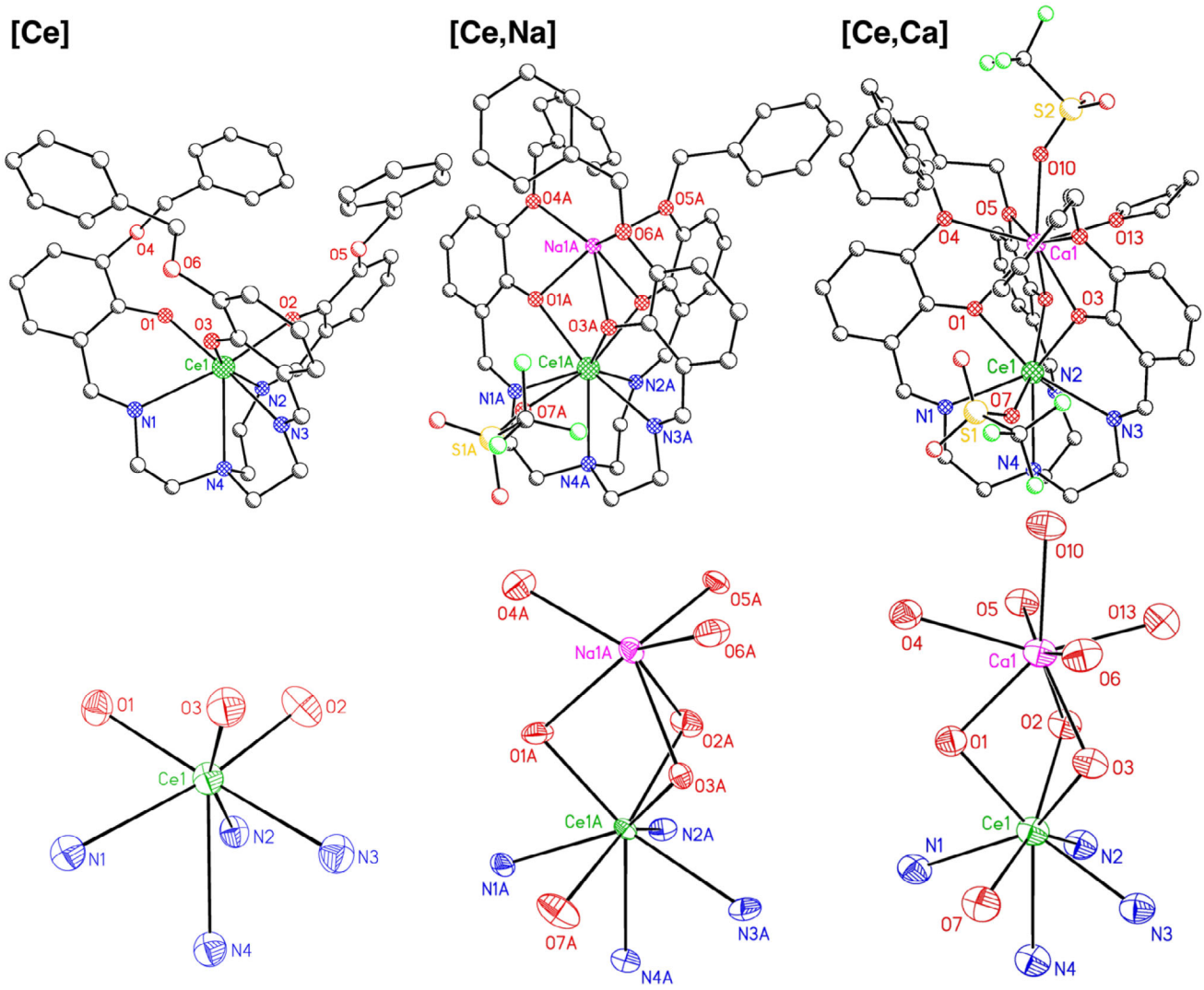

Figure 2. Solid-state structures of **[Ce]**, **[Ce,Na]**, and **[Ce,Ca]** from XRD analysis. O7A in the structures of **[Ce,Na]** and O7 and O10 in the structures of **[Ce,Ca]** are associated with κ^1-triflate moieties, while O13 in the structure of **[Ce,Ca]** is associated with a bound tetrahydrofuran molecule. In the upper structures, the metals and first-sphere ligand atoms are shown with cross-hatched circles, and all other atoms are shown with shaded circles. In the lower structures, displacement ellipsoids are shown at the 50% probability level for only the metals and first-sphere ligand donor atoms. All hydrogen atoms, outer-sphere solvent molecules, and a second co-crystallized molecule of **[Ce,Na]** are omitted for clarity.

from the solution-state characterization. With respect to the packing of **[Ce]**, no π-π interactions were measurable, though weak electrostatic interactions between O1 and H12 of an adjacent **[Ce]** molecule could be quantified which likely influence the long-range order of the structure (see Supporting Information, Figure S41). Although the two independent isomers are found in the solid state, **[Ce]** can be anticipated to rapidly interconvert between the Δ and Λ forms in the solution phase on the basis of NMR analysis (vide supra).[47] Thus, the *quasi*-C_3 symmetry of the complex in the solid state is consistent with the solution-phase effective C_3 symmetry.

Designating the three oxygen and four nitrogen atoms bonded directly to Ce as vertices of a polyhedron reveals a *quasi*-monocapped trigonal antisprismatic geometry about the Ce center in **[Ce]** (see Supporting Information, Figure S64). The identity of the coordination polyhedron is confirmed by the measured twist angle (Θ), defined here as the average dihedral angle between an imine nitrogen of a given arm of the ligand, the centroid of the imine nitrogen plane composed of N1, N2, and N3, the centroid of the phenoxide plane composed of O1, O2, and O3, and a phenoxide oxygen on the same arm as the original imine nitrogen. In the case of **[Ce]**, we measured Θ to be +45.3°, which is consistent with a *quasi*-monocapped trigonal antiprismatic polyhedron, as a perfect trigonal antiprism (octahedron) would display a value of +60° (see Supporting Information, Figure S69). A related twist angle (Θ') can also be measured for the oxygen atoms composing the upper hexadentate site which reveals a *quasi*-trigonal prismatic geometry in the case of **[Ce]** on the basis of the value $\Theta' = -14.8$ °(an ideal trigonal prism would display a Θ' angle of 0°).

The interatomic phenoxide and imine distances also highlight the properties of the coordination environment around Ce. The oxygen atoms that compose the top face of the polyhedron (O1–O3) display average interatomic distances of 3.448(3) Å,

Table 1. Selected average bond lengths, interatomic distances, pK_a values of $[M(H_2O)_m]^{n+}$, and Shannon Ionic Radii.[48]

	[Ce]	[Ce,Na][e]	[Ce,Ca]
pK_a of $[M(H_2O)_m]^{n+}$	–	14.8	12.6
Shannon Ionic Radius of M (Å)[a]	–	1.02	1.12
C.N. of Ce	7	8	8
C.N. of M	–	6	8
Θ (°)[b]	+45.3	+10.4	+5.5
Ce-O_{Ar} (Å)[f]	2.299(2)	2.341(12)	2.394(3)
Ce-N_{imine} (Å)[f]	2.604(3)	2.645(15)	2.609(4)
Ce-N4 (Å)[f]	2.802(3)	2.706(13)	2.733(4)
N-C_{imine} (Å)	1.284(5)	1.297(20)	1.283(6)
M–O_{Ar} (Å)[f]	–	2.381(14)	2.406(3)
M-O_{Ether} (Å)[f]	–	2.475(14)	2.570(3)
Ce•••M (Å)	–	3.344	3.547
O_{Ar}•••O_{Ar} (Å)[c,f]	3.448(3)	2.877(18)	2.793(4)
O_{Ether}•••O_{Ether} (Å)[d,f]	6.391(4)	3.955(17)	4.103(4)

[a] Average radii observed for cation-anion distances in oxide and fluoride crystal structures; see reference [48].
[b] The twist angle of the heptadentate site (θ) is defined as the average dihedral angle between the phenoxide O atom, the center-of-gravity of the phenoxide oxygen plane (CGO1), the center-of-gravity of the imine nitrogen plane (CG3N), and the imine N atom for each ligand arm. For each arm, Θ(O-CGO1-CG3N-N) represents the angle between vector O-CGO1 and vector CG3N-N when viewed down vector CGO1-CG3N. Θ is positive if O-CGO1 is rotated clockwise onto CG3N-N. See Supporting Information, p. S64 for details.
[c] Average distance between the O1, O2, and O3 atoms in the plane defined by the phenoxide moieties.
[d] Average distance between the O4, O5 and O6 atoms in the plane defined by the aryl ether moieties.
[e] Average values are given that consider both of the molecules in the unit cell of the structure of [Ce,Na]. Values for both molecules present in the unit cell, along with relevant average and estimated variance data, are listed in the Supporting Information Table S2.
[f] The value in parentheses refers to the E.S.D. that is the largest for an individual entry among the independent values used to compute the average.

which are longer than the sum of the Van der Waals' (VdW) radii (2.8 Å) for each given pair of O atoms by ca. 0.65 Å. Staggered below them, the nitrogen atoms (N1–N3) also display average interatomic distances (4.098(4) Å) which are longer than the sum of their VdW radii (3.0 Å) by more than an angstrom. This extended length of the interatomic distances for N1–N3 (compared to the sum of their VdW radii) can be assigned to arise principally from the presence of the capping N4 atom, which effectively pushes the other nitrogen atoms away from each other.

XRD analysis of **[Ce,Na]** and **[Ce,Ca]** confirmed the binding of each secondary metal cation in the hexadentate site provided by the ligand, while also retaining the Ce^{3+} center in the lower site (Figure 2). Selected bond metrics are provided in Table 1 and crystallographic details are given in the Supporting Information (see Supporting Information, pp. S34–S58). The binding of the eighth ligand in the structures of **[Ce,Na]** and **[Ce,Ca]** disrupts the previous *quasi*-C_3 symmetry found for **[Ce]** and results in *quasi*-C_s symmetry. In addition to the presence of the eighth ligand, the symmetry of **[Ce,Ca]** is further broken by a weak electrostatic interaction which orients one of the benzyloxy groups down toward the triflate anion that is bound to Ce (see Supporting Information, Figure S62). Similar to the case of **[Ce]**, no π-π interactions are observed, but the packing of both **[Ce,Na]** and **[Ce,Ca]** are influenced by weak electrostatic interactions (see Supporting Information, Figures S50 and S63).

Drastic structural changes take place upon the binding of the secondary metal cation, the most obvious being the binding of an eighth ligand to the Ce center (an oxygen atom from a triflate anion in both cases). This additional ligand, denoted $\mathbf{L^m}$, coordinates to the Ce through the face formed by O1, O3, N1, and N3 and changes the coordination environment of Ce from a *quasi*-monocapped trigonal antiprism to a dodecahedron, similar to the behavior observed previously for related high coordination number structures (see Supporting Information, Figure S65).[30,32,34] The space needed for the binding of $\mathbf{L^m}$ to the previously seven-coordinate Ce center arises from the contraction of the O_{Ar}•••O_{Ar} interatomic distances. The O_{Ar} atoms are drawn together to form a shared (intermetallic) triangular-shaped polyhedral face upon coordination of the secondary Lewis acidic metal cation (see Supporting Information, Figures S66 and S67). In the case of the phenoxide oxygens (O1–O3), the average interatomic distances (2.877(17) Å for **[Ce,Na]** and 2.788(4) Å for **[Ce,Ca]**) contract such that they are close to the sum of the VdW radii (2.8 Å), while the average aryl ether interatomic distances also contract upon secondary cation binding. However, the average inter-ether distances remain longer, likely due to the steric crowding of the benzyloxy groups around the upper cavity (3.955(17) Å for **[Ce,Na]** and 4.103(4) Å for **[Ce,Ca]**). Collectively, this contraction of the O_{Ar}•••O_{Ar} and O_{ether}•••O_{ether} distances engendered by the presence of the secondary metal cation serves to open up the distances between O1, O3, N1, and N3 on the cerium coordination polyhedron, thereby forming an accessible trapezoidal face that allows $\mathbf{L^m}$ to bind to the Ce center. The longitudinal positioning of the eighth ligand $\mathbf{L^m}$ is dictated by the presence of the three arms of $\mathbf{L^{OBn}}$, which contains sufficiently rigid motifs between the N_{imine} atoms and O_{Ar} atoms (as well as between N4 and the N_{imine} atoms) such that the available binding site is along the edges of the N_{imine}•••N_{imine} plane. Consistent with these changes, a drastic decrease is measured in the twist angle Θ to values of +10.4° and +5.5° for **[Ce,Na]** and **[Ce,Ca]**, respectively, compared to that of **[Ce]** (see Supporting Information, Figure S69).

The compounds presented here and the analogous ethoxy-substituted complexes afford the unique opportunity to distinguish effects of steric bulk versus Lewis acidity of a secondary metal on the structural organization about Ce as they offer a set of common structural features. The structural phenomena, coordination environment, and metrics of **[Ce]**, **[Ce,Na]**, and **[Ce,Ca]** mimic those observed for the related tripodal Ce^{3+} complexes reported by our group which feature ethoxy-substituted ligand arms rather than benzyloxy.[30] The foregoing structural details described for the family of complexes presented here offer a useful accompaniment to the analysis of polyhedral features and structural analysis of tuning effects presented for the ethoxy

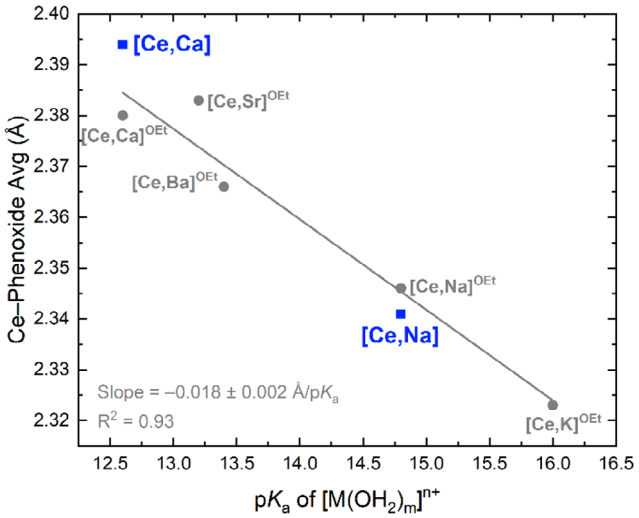

Figure 3. Dependence of the average Ce–O_{Ar} distance in **[Ce,Na]** and **[Ce,Ca]** on the pK_a of $[M(H_2O)_m]^{n+}$ compared to the metrics of the companion ethoxy complexes in gray.[30]

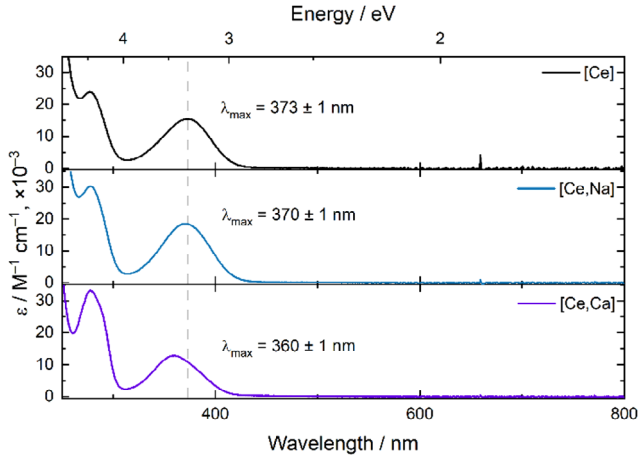

Figure 4. Electronic absorption spectra of **[Ce]**, **[Ce,Na]**, and **[Ce,Ca]** in THF.

complexes, in that the metrics measured and computed for **[Ce]**, **[Ce,Na]**, and **[Ce,Ca]** appear to follow the same trends in structural tuning. In this jointly applicable model, the ionic radius of the secondary metal cation dictates the positioning of the secondary metal cation in the hexadentate site provided by the six oxygen donors of the ligand, where smaller cations can reside closer to the bridging phenoxide donors. The position of the Ce center, however, is governed by the charge density of the secondary cations, quantified here by the pK_a values of the metal-aquo ions ($[\mathbf{M}(H_2O)_m]^{n+}$), where more Lewis acidic cations push the Ce lower in the heptadentate site.

These two contributions can be delineated by quantifying the longitudinal displacement and angular positions of the Ce^{3+} center and the secondary metal cation (M^{n+}) relative to the centroid between the two metals (see Supporting Information, Figures S79 and S80).[30] Aside from the general trends of such metrics with the pK_a values and ionic radii of the secondary metal cations, a close inspection of the displacement of the secondary metal cations in the ethoxy and benzyloxy compounds reveals that the increased steric bulk of the benzyloxy groups appears to push the Lewis acidic metal centers slightly closer to the phenoxide core while also pushing the Ce centers away from the phenoxide core compared to their positions in the ethoxy complexes. In line with this movement, the average O_{Ar}-Ce-X1B angles contract and the O_{Ar}-**M**-X1B angles slightly expand in the benzyloxy complexes relative to their ethoxy counterparts (see Supporting Information, Figures S81 and S82; X1B is the center of gravity of the 3O triangle containing O1, O2, and O3).

Overlaying the Ce–O_{Ar} distances of **[Ce,Na]** and **[Ce,Ca]** with those of the family of ethoxy complexes shows that the benzyloxy system follows the shared model of phenoxide-mediated communication as a function of Lewis acidity (see Figure 3). Notably, **[Ce,Na]** and **[Ce,Ca]** deviate from the ethoxy complexes in opposite directions, likely a result of the bulky benzyloxy groups which are able to arrange themselves tightly in a *quasi*-C_3-symmetric fashion in **[Ce,Na]** but which bend further outwards in **[Ce,Ca]**. The outward bend represents a further distortion of the structure of **[Ce,Ca]** (vide supra). Taken together, structural effects of cation incorporation and ligand modification both appear to impact the electronic communication provided by the phenoxide ligands that bridge between Ce and **M**. Seeing this, cation binding could be safely anticipated to modulate the structural, spectroscopic, and electrochemical properties of the complexes as well.

2.3. Electronic Absorption Spectroscopy

Electronic absorption spectroscopy was used to probe the effects of the secondary cations on the electronic properties of **[Ce]** in THF (see Figure 4). In the case of **[Ce]**, two strong absorptions were measured between 200 and 300 nm which are likely associated with intraligand transitions of $\mathbf{L^{OBn}}$ on the basis of their high molar absorptivity values (ε_{243nm} = 65,900 M^{-1} cm^{-1}; ε_{277nm} = 24,000 M^{-1} cm^{-1}). An additional feature can be seen at 373 ± 1 nm (ε_{373nm} = 15,640 M^{-1} cm^{-1}) which likely corresponds to mixed charge-transfer (CT) and *4f*→*5d* transitions of the Ce^{3+} center, as observed in other complexes of Ce^{3+}.[30,49] In certain coordination environments, unique *4f*→*5d* transitions can be observed for Ce^{3+} and these typically display molar absorptivity values less than 1000 M^{-1} cm^{-1}. Thus, the transitions observed here are likely mixed with more strongly absorbing CT transitions.[50–52]

An overall shift to higher energies was observed for the CT transition going from **[Ce]** to **[Ce,Ca]** (from 3.32 eV to 3.44 eV). The magnitude of this shift is similar to that reported for the ethoxy-substituted analogues.[30] However, the energies of the individual highlighted transitions measured for **[Ce]**, **[Ce,Na]**, and **[Ce,Ca]** are lower for the benzyloxy complexes than the ethoxy complexes (see Supporting Information, Figure S28). At this stage, we anticipate that there are two possible explanations for the shift of the noted transitions to lower energy for the complexes ligated by $\mathbf{L^{OBn}}$. The crystallographic data showing closer placement of the incorporated secondary cations near the phenoxide moieties in the complexes ligated by $\mathbf{L^{OBn}}$ could be linked

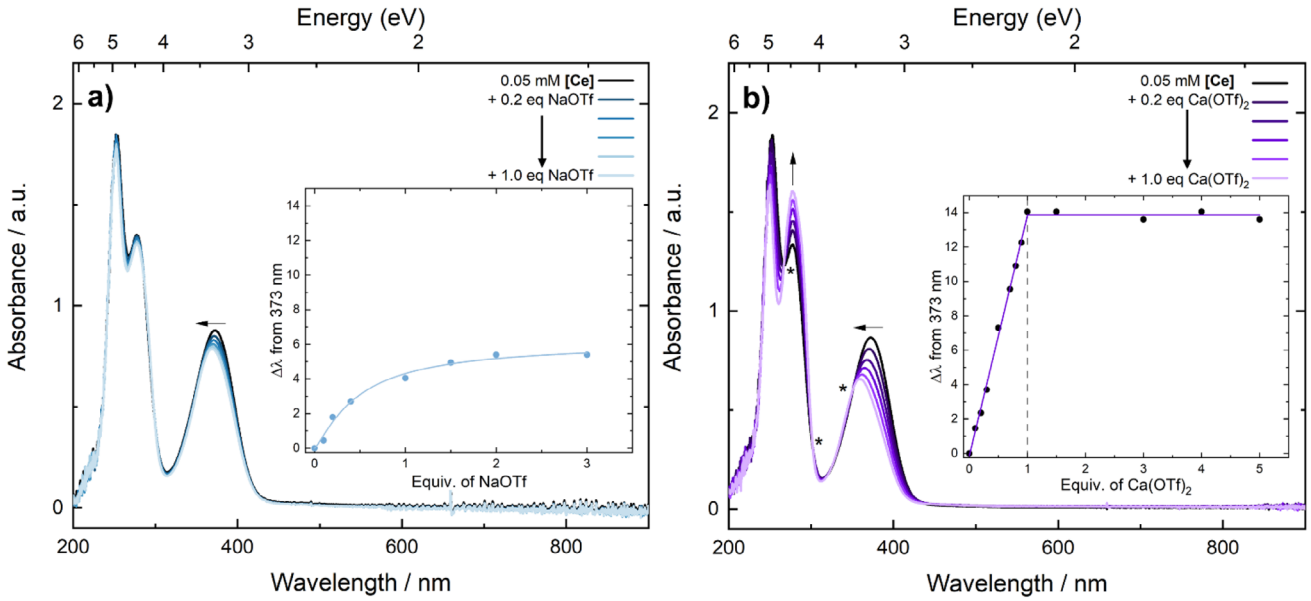

Figure 5. Electronic absorption spectra corresponding to titrations of **[Ce]** with (a) NaOTf and (b) $Ca(OTf)_2$ in THF. Isosbestic points are indicated by asterisks, and insets show the shift in the absorption maxima versus the equivalents of metal triflate salt added.

to enabling the Lewis acidic metals to exert a stronger influence on the acceptor orbitals found on the phenoxide moieties and thereby drive the blue shifting of the CT component of the transitions. Alternatively, the additional conjugated phenyl rings of $\mathbf{L^{OBn}}$ could support delocalization of charge following excitation; this could also serve to red-shift the peak maxima as measured.

2.4. Binding Studies of $M^{n+}(OTf)_n$ Salts to [Ce]

Close inspection of the electronic absorption spectrum of **[Ce,Na]** reveals that a smaller shift (3 ± 1 nm) in the absorption maximum of the CT transition is observed for **[Ce,Na]**, compared to 6 ± 1 nm in the case of $\mathbf{[Ce,Na]^{OEt}}$.[30] This indicated to us that there could be a difference in the binding affinity for secondary cations of the benzyloxy complexes compared to the ethoxy complexes. Thus, we conducted titration experiments in THF with UV-visible detection to interrogate the propensity for **[Ce]** to bind our chosen metal triflate salts. Titration experiments were performed in THF, as opposed to acetonitrile (MeCN; utilized in synthesis), because **[Ce]** is not sufficiently soluble in MeCN.

Addition of sodium triflate to **[Ce]** in THF resulted in a gradual shift of the transition (with both CT and *4f→5d* character, vide supra) located initially near 373 nm. Over the course of the titration, the absorption maximum of the noted transition shifted by ca. 6 nm with no true isosbestic points measured in the spectra (see Figure 5a). In contrast, the addition of calcium triflate to **[Ce]** in THF resulted in several isosbestic points at λ_{iso} = 267, 302, and 350 nm, indicating a tight binding of Ca^{2+} and the clean formation of a single new species. Indeed, the data points up to 1 eq. of the $Ca(OTf)_2$ titration fit a straight line very well (R^2 = 0.997; y-intercept restrained to zero; see Figure 5b). The data points beyond 1 eq. also display high linearity and a small error on the y-intercept (13.9 ± 0.1; slope restrained to zero), indicating that no additional Ca^{2+} ions associate with **[Ce]** beyond a 1:1 ratio. Finally, the molar absorptivity at 360 nm (determined in situ at the conclusion of the titration) for a 1:1 combination of **[Ce]** and $Ca(OTf)_2$ is 13 151 M^{-1} cm^{-1} which is in reasonable agreement with the molar absorptivity of isolated **[Ce,Ca]** (12 710 ± 60 M^{-1} cm^{-1}; error on the molar absorptivity is the error on the slope of Beer's Law plot for **[Ce,Ca]**).

In the titration with Na^+, the shift in absorption maximum displays a nonlinear, asymptotic approach toward a maximum value which lies beyond 1 equivalent of added Na^+. This is likely indicative of a reversible binding equilibrium, contrasting with the strong, irreversible binding observed for Ca^{2+} (vide supra). We anticipate that the 1:1 binding isotherm[53] does not fit the Na^+ data well (see Supporting Information, Figure S29) because of the possibility that multiple sodium cations could interact simultaneously with the upper site; interaction of the first Na^+ equivalent is expected to be most preferred, but more could in principle interact as well. Nevertheless, the equilibrium binding behavior of Na^+ to **[Ce]** can be described by the Hill-Langmuir equation[54] (despite anticipated minor effects from dilution, shown in the inset of Figure 5a), which gives an α value of 1.2 ± 0.2; this is suggestive of a near 1:1 ratio of Ce:Na at saturation, along with some propensity of binding additional Na^+ as mentioned above. Consistent with a reversible binding scenario for Na^+, $\Delta\lambda$ at 1 eq. of Na^+ is only at ca. 66% of $\Delta\lambda_{max}$, which represents the maximum shift as extracted from the Hill-Langmuir fit (see Supporting Information, Figure S30). The equilibrium binding of Na^+ to **[Ce]** in THF observed spectrophotometrically could be derived from similar solvation/coordination environments provided by the ether oxygens of THF solvent molecules compared to the hexadentate binding site of **[Ce]** which includes 3 benzyloxy (i.e., benzyl ether) groups. **[Ce,Na]** forms readily in MeCN in high yield and gives rise to high-quality single crystals

with diethyl ether as a crystallization co-solvent (the same conditions used to bulk recrystallize **[Ce,Na]** for elemental analysis, which was satisfactory).

The stronger affinity of **[Ce]** for Ca^{2+} and the ability of Ca^{2+} to induce a larger shift in the noted electronic transition are both consistent with the higher charge density and greater Lewis acidity of Ca^{2+}. In related studies by our group of 2D crown ether and "tiara" complexes, tight binding in a 1:1 ratio was observed for multiple monovalent ions of various sizes (Li^+ to K^+), with the exception of the quite charge diffuse Cs^+ ion.[21] In these cases, an 18-crown-6-like moiety or two related tridentate neutral O-donor moieties served as the binding site for the cations and virtually identical binding behavior/affinity was observed. Though these 2D compounds are conceptually similar to the tripodal 3D compounds studied here and could be expected to display similar tight binding behavior, differences are apparent from the titration experiments. One possible reason for the observation of weaker binding toward Na^+, despite the hexadentate upper cavity provided by **[Ce]** serving as a voracious and flexible acceptor of cations, lies in the significant structural rearrangement that takes place in the benzyloxy complexes upon binding a cation. The 2D ligands undergo much less structural rearrangement in their phenoxide-containing cores upon binding a cation than the benzyloxy compounds on the basis of XRD. For example, the $O_{Ar}\bullet\bullet\bullet O_{Ar}$ distance of **[Ni]**^{T} (the monometallic Ni^{II} tiara complex) contracts by 0.012 Å to accommodate a K^+ ion and 0.030 Å to accommodate a Sr^{2+} ion,[21] whereas the average $O_{Ar}\bullet\bullet\bullet O_{Ar}$ distance of **[Ce]** must contract by 0.571 Å to accommodate a Na^+ ion and 0.655 Å to accommodate a Ca^{2+} ion. These contractions are similar to those measured for **[Ce,Na]**^{OEt} and **[Ce,Ca]**^{OEt}, which display average $O_{Ar}\bullet\bullet\bullet O_{Ar}$ contractions of 0.524 Å and 0.597 Å, respectively, relative to **[Ce]**^{OEt}.[30] The observation of weaker binding of Na^+ by **[Ce]** is likely a result of greater structural rearrangement upon cation binding, which would indeed be exaggerated compared to the ethoxy complexes by the increased steric bulk of the benzyloxy groups and the ability of the benzyloxy groups to push the secondary cation closer toward the phenoxide bridge and cerium center. Nevertheless, the phenoxide moieties still serve the crucial role of enabling the tuning effects of the cations on the Ce^{3+} center by facilitating electronic communication. The facilitation of electronic communication in the tripodal $\mathbf{L}^{OBn}$ and $\mathbf{L}^{OEt}$ ligand systems is also similar to effects encountered in a 2D crown ether ligand supporting redox-active vanadyl complexes.[23]

2.5. Electrochemical Studies

With structural and spectroscopic characterization in hand, we next investigated the electrochemical properties of the synthesized Ce(III) complexes (Figure 6). Cyclic voltammetry data for **[Ce]** in THF-based electrolyte show a single accessible redox event when sweeping anodically at $E_{1/2} = -0.40$ V (all potentials quoted versus ferrocenium/ferrocene, denoted $Fc^{+/0}$). Both the oxidized and reduced forms of the complex appear to be freely diffusional in solution on the basis of scan rate-dependent data (see Supporting Information, Figure S32), and the $Ce^{IV/III}$ couple of **[Ce]** appears to be *quasi*-reversible on the basis of its peak-to-peak separation (ΔE_p) of 131 mV measured at a scan rate of 100 mV/s (ΔE_p of ferrocene measured on the same day and under the same conditions was 141 mV). Cyclic voltammetry data for bulk-prepared samples of **[Ce,Na]** and **[Ce,Ca]** dissolved in THF electrolyte reveal similar *quasi*-reversible $Ce^{IV/III}$ couples that are shifted to more positive potentials compared to **[Ce]** at $E_{1/2}$ = -0.34 V and 0.23 V (Table 2), respectively, as a result of the influences engendered by the Lewis acidic secondary metal cations. The heterogeneous electron transfer rates for the redox process of both **[Ce,Na]** and **[Ce,Ca]** appear to be slower compared to **[Ce]** on the basis of their broadened wave shapes and increased ΔE_p values of 174 and 212 mV, respectively; slow electron transfer kinetics have been documented in a variety of systems for the $Ce^{IV/III}$ couple and represent a key variable in the electrochemistry of Ce complexes.[9] Nevertheless, scan rate-dependent data for both couples indicate that both the reduced and oxidized forms of **[Ce,Na]** and **[Ce,Ca]** are freely diffusional in solution (see Supporting Information, Figures S34 and S36).

With the goal of this study to interrogate the effects of ligand modification and Lewis acid incorporation on the structural

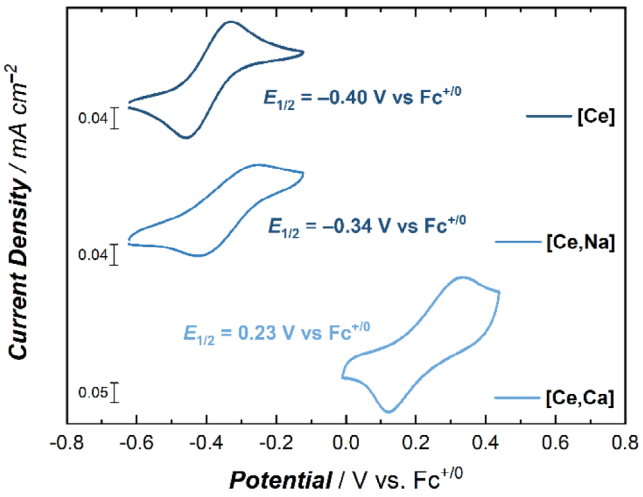

Figure 6. Cyclic voltammetry data for **[Ce]**, **[Ce,Na]**, and **[Ce,Ca]** in THF electrolyte. Electrolyte: 0.1 M [^{n}Bu$_4$N][PF$_6$] in THF; scan rate: 100 mV/s; **[Ce]** = 0.5 mM, **[Ce,Na]** = 0.5 mM, **[Ce,Ca]** = 1.68 mM.

Table 2. Electrochemical parameters.

	[Ce]	[Ce,Na]	[Ce,Ca]
pK_a[a]	–	14.8	12.6
Conc. of complex (mM)	0.5	0.5	1.68
$E_{1/2}$ **(V vs Fc$^{+/0}$)**	−0.40	−0.34	0.23
$\Delta E_{1/2}$ **([Ce,M]–[Ce]) (V)**[b]	–	+0.06	+0.63
ΔE_p **(mV)**[c]	131	174	212

[a] pK_a values taken from ref. [13].
[b] Defined as the difference in the midpoint potential of **[Ce,M]** and **[Ce]**.
[c] Defined as the difference between the anodic and cathodic peak potentials; values quoted at a scan rate of 100 mV/s.

and redox properties of Ce^{3+} in mind, it is useful to make comparisons to the related **[Ce]**^{OEt} and **[Ce,M]**^{OEt} complexes.[30] Both monometallic Ce^{3+} complexes display similar electrochemical profiles, with *quasi*-reversible couples in THF-based electrolyte at $E_{1/2} = -0.43$ V for **[Ce]**^{OEt} ($\Delta E_p = 125$ mV; see Supporting Information, Figure S37) and -0.40 V for **[Ce]**. **[Ce]**^{OEt} displays a more negative reduction potential than **[Ce]**, likely a result of the tighter coordination of the phenoxides to Ce^{3+} enabled by the less sterically bulky ethoxy substituents. Alternatively, the expected difference in electron-donating/withdrawing characteristics between the ethoxy and benzyloxy substituents could contribute to the measured shift in reduction potential; such an effect would be attributable to the conjugated nature of the additional phenyl rings present in **[Ce]**.

A more significant difference, however, is encountered when comparing the magnitude of the measured shift in $E_{1/2}$ between the monometallic complexes and the Ce•Na bimetallic complexes of each tripodal ligand. In the case of **[Ce]**^{OEt} and **[Ce,Na]**^{OEt}, the $\Delta E_{1/2}$ between the monometallic and sodium heterobimetallic complexes is +170 mV, whereas a modest shift of only +60 mV was measured here between **[Ce]** and **[Ce,Na]**. The smaller $\Delta E_{1/2}$ observed for **[Ce,Na]** is consistent with the hypothesis that the Na^+ cation is less tightly bound than in **[Ce,Na]**^{OEt} (as well as less tightly bound than Ca^{2+} in **[Ce,Ca]**). In this scenario, the steric bulk of the benzyloxy substituents effectively decreases the binding affinity for the less Lewis acidic Na^+ ion such that it participates in a reversible equilibrium, precluding it from exerting its full influence over the Ce^{3+} center and shifting the $Ce^{IV/III}$ couple by the expected amount. Despite the modest $\Delta E_{1/2}$ observed for **[Ce,Na]**, the greater effect of the highly Lewis acidic Ca^{2+} ion on the $Ce^{IV/III}$ redox is apparent in the voltammetry of **[Ce,Ca]**. A $\Delta E_{1/2}$ of +630 mV was measured for **[Ce,Ca]** with respect to **[Ce]** in THF-based electrolyte, which is virtually identical to the magnitude of the shift observed for **[Ce,Ca]**^{OEt} ($\Delta E_{1/2} = 630$ mV; measured in MeCN-based electrolyte).[30]

Taken together, these data highlight the ability to tune the redox chemistry of high coordination number metals, such as Ce, by the incorporation of Lewis acidic secondary metal cations and demonstrate the effects of steric ligand modifications on the properties of the complexes. Although the influence of tightly binding metal ions on electron transfer and reactivity has been well documented for transition metal complexes,[55–57] the effect of binding thermodynamics on such properties is less studied for transition metal species and unknown for complexes containing redox-active lanthanides.[58] Importantly, the equilibrium binding of Na^+, as measured in the spectrochemical titrations, affects the resulting electrochemical tuning behavior–equilibrium binding results in only a partial tuning effect compared to what is achievable when the cation is tightly bound to the same or a similar receptor site.

3. Discussion

Prior studies by our group and others have highlighted the usefulness of Schiff-base and ether motifs for the purpose of encapsulating two metals in close proximity to each other, which has enabled study of the structural, spectroscopic, and electrochemical properties of redox processes as influenced by secondary metal cations. We have only recently[30] ventured into investigations of high coordination number metals, such as cerium(III), which required modification of our preferred type of ligand framework to include both a third "arm" for lanthanide binding and capping ethoxy groups to form an upper site for secondary cation binding. Development of this ligand, denoted $\mathbf{L}^{OEt}$, has proven useful, however, as $\mathbf{L}^{OEt}$ affords stereochemical control over cation binding and largely avoids problems which could impact study of high coordination number systems.[30] Here, we modified the composition of $\mathbf{L}^{OEt}$ by substituting the ethoxy moieties for benzyloxy groups to interrogate the interplay of ligand modifications and the incorporation of Lewis acidic metal cations. Overall, we have found that the primary difference in solution chemistry resulting from this structural modification is a marked decrease in the binding affinity of the upper hexadentate site for Na^+. The weak binding of Na^+ was observed both spectroscopically and electrochemically. Notably, the reversible equilibrium binding scenario of Na^+ to **[Ce]** did not prelude the detection of a tuning effect via spectroscopic, electrochemical, and structural means, indicating that tight binding of a secondary Lewis acidic metal cation is not necessarily essential to achieve tuning of the properties of a complex. However, tight binding can be confidently concluded to be required for achievement of the maximal tuning shift for a binding site—given that the results here show that only a smaller, fractional shift is accessible when the cation (tuning agent) is dynamically moving in and out of the site designed to engender communication with the metal center desired for tuning.

At this stage, a positive shift in reduction potential can be reasonably expected upon incorporation of secondary Lewis acidic metal cations to any suitable redox-active complex. Similar to the previously studied cerium complexes featuring ethoxy groups,[30] the range of the shift encountered here, which spans 630 mV, is larger than those measured for transition-metal-containing or uranyl-containing bimetallic complexes studied by our group. This is made possible by the presence of the three bridging phenoxide donor atoms, which compose the critically important shared triangular face between the coordination polyhedra of the Ce^{3+} center and the secondary cations. The presence of this shared triangular face can be safely concluded to provide the enhanced electrostatic "communication" between metal centers that underpins large shifts in reduction potentials.

Notably, the bimetallic **[Ce,Na]** and **[Ce,Ca]** complexes display more negative reduction potentials than their ethoxy-substituted counterparts (Figure 7). However, as the electrochemical data for the series of benzyloxy-substituted complexes were collected in THF-based electrolyte and the data for the ethoxy-substituted complexes was collected in MeCN-based electrolyte, detailed comparisons between these data sets could be reflective of solvation differences rather than intrinsic molecular features and are thus not discussed further. With this caveat in mind, however, approximating a fit of the two benzyloxy data

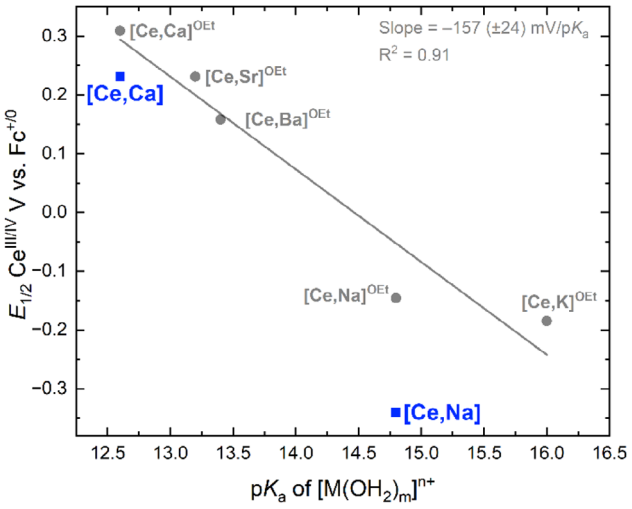

Figure 7. Correlation of the $Ce^{IV/III}$ $E_{1/2}$ values of **[Ce,Na]** and **[CeCe]** on the Lewis acidity (pK_a) of the corresponding $[M(H_2O)_m]^{n+}$ complexes compared to the metrics of the companion ethoxy complexes in gray.[30]

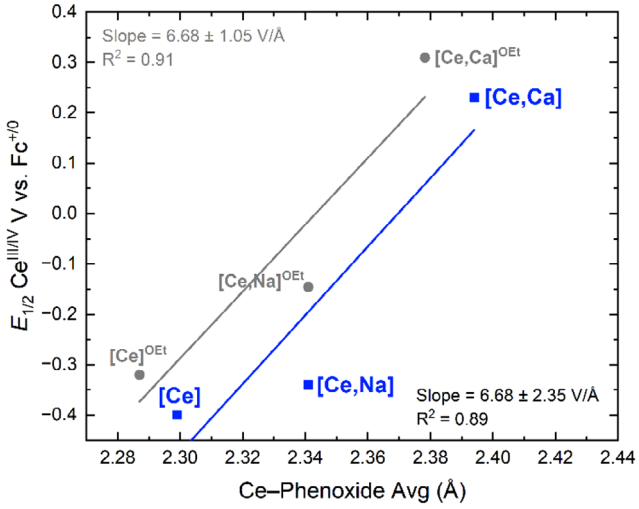

Figure 8. Dependence of the $Ce^{IV/III}$ reduction potential for the complexes in this study (measured in THF) on the average Ce–phenoxide distances compared to the metrics of the companion ethoxy complexes in gray.[30] Reduction potentials of the complexes featuring ethoxy substituents were measured in MeCN.

points with a linear fit of the same slope of that observed for the **[Ce,M]^{OEt}** complexes reveals reasonable co-linearity between the cation-driven tuning effects observed in the two ligand systems (see Supporting Information, Figure S38). Notably, the y-intercept of the line approximating the trend in the benzyloxy complexes is offset by -0.18 V from the y-intercept of the line fit to the ethoxy data, showing that the electrochemical tuning range achieved through the small ligand adjustment explored here is less drastic than that achieved by incorporation of Lewis acidic metal cations.

Consistent with the structural tuning model put forth in our prior work,[30] the position of the Ce atom in the lower heptadentate compartment of the ligand relative to the plane formed by the three phenoxides is governed by the Lewis acidity of the secondary cation, while the position of the secondary cation relative to this plane is dictated by the ionic radius of the secondary cation. Clear evidence for the relation of the structural and electrochemical tuning effects to the Lewis acidity of the secondary cations can be found in the linear relationships between the $E_{1/2}$ of the $Ce^{IV/III}$ complexes and the average Ce–phenoxide distances (Figure 8). Comparing each benzyloxy complex with its ethoxy counterpart shows variability attributable to the subtle effects induced by the bulky benzyloxy moieties. Nevertheless, the underlying driving force for the changes observed in the structural, spectroscopic, and electrochemical behavior of the Ce complexes in these two families is the same: the Lewis acidity of the secondary metal cation modulates properties of the Ce^{3+} center through the bridging phenoxide atoms. However, this work shows that the sterically demanding benzyl groups can serve to "push" the bound secondary cation toward the critical shared triangular polyhedral face, resulting in particular changes in the structural metrics for the complexes that are consistent with the influence of cation-cation repulsion on the properties of the heterobimetallic complexes studied here.

4. Conclusion

We have prepared a family of tripodal complexes which are able to accommodate Ce^{3+} in a high coordination environment, as well as bind a second metal cation for the modulation of the complexes' overall properties. An attenuation of the binding affinity of the hexadentate binding pocket for Lewis acidic metal cations was measured and compared to behaviors encountered with a previously studied family of Ce complexes containing ethoxy substituents instead of benzyloxy groups. Evidence for clear points of difference induced by the controlled change in ligand structure was found in both the spectroscopic and electrochemical data. Despite the difference in binding affinity for the weakly Lewis acidic Na^+, a rather large shift in the $Ce^{IV/III}$ redox potential of 630 mV resulted from the incorporation of Ca^{2+} into the monometallic cerium complex. Measured cation-induced structural changes are consistent with the unified structural model described both here and in our prior work,[30] providing evidence that our structural model appears broadly applicable to complexes of the general type discussed here. Overall, this study highlights the effects that a small but controlled ligand modification can have on the properties of complexes of high coordination numbers compared to the effects of Lewis acid incorporation as well as the robust point of connection that can tie together structural insights from crystallographic analysis and practically achievable solution chemical properties.

5. Experimental Section

5.1. General Considerations

All manipulations were carried out in dry N_2-filled gloveboxes (Vacuum Atmospheres Co., Hawthorne, CA) or under N_2 atmosphere

using standard Schlenk techniques unless otherwise noted. All solvents were of commercial grade and dried over activated alumina using a PPT Glass Contour (Nashua, NH) solvent purification system prior to use and were stored over molecular sieves. $Ce(N(SiMe_3)_2)_3$ was prepared according to literature procedure and purified by recrystallization, though a small impurity of bis(trimethylsilyl)amine persisted.[30,59] However, this impurity of bis(trimethylsilyl)amine could be readily removed from the isolated **[Ce]** product of the subsequent ligand-metalation reaction. All chemicals were from major commercial suppliers and used as received. CD_3CN and CD_2Cl_2 were purchased from Cambridge Isotope Laboratories and dried over 3 Å molecular sieves and calcium hydride, respectively. ^1H, ^{13}C, and ^{19}F NMR spectra were collected on 400 and 500 MHz Bruker spectrometers and referenced to the residual protio-solvent signal in the case of ^1H and ^{13}C.[60] ^{19}F NMR spectra were referenced and reported relative to CCl_3F as an external standard following the recommended scale based on ratios of absolute frequencies (Ξ).[61,62] Chemical shifts (δ) are reported in units of ppm and coupling constants (J) are reported in Hz. Electronic absorption spectra were collected with an Ocean Optics Flame spectrometer, in a 1-cm path length quartz cuvette. Experimental high-resolution mass spectrometry data were collected on an LCT Premier mass spectrometer equipped with a quadrupole, time-of-flight mass analyzer, and an electrospray ion source. Predicted mass spectrometry data were obtained from PerkinElmer Informatics' ChemDraw Professional Suite.

5.2. Elemental Analysis

Elemental analyses were performed at the CENTC Elemental Analysis Facility at the University of Rochester. Microanalysis samples were weighed with a PerkinElmer Model AD6000 Autobalance, transferred under argon, and combusted in a tin capsule that was crip-sealed with a die apparatus. Air-sensitive samples were handled in a VAC atmospheres glovebox and their compositions were determined by a PerkinElmer 2400 Series II analyzer.

5.3. Electrochemistry

Electrochemical experiments were carried out in a nitrogen-filled glove box. 0.10 M tetra(n-butylammonium) hexafluorophosphate (Sigma-Aldrich; electrochemical grade) in acetonitrile served as the supporting electrolyte. Measurements were made with a Gamry Reference 600 Plus Potentiostat/Galvanostat using a standard three-electrode configuration. The working electrode was the basal plane of highly oriented pyrolytic graphite (HOPG) (GraphiteStore.com, Buffalo Grove, Ill.; surface area: 0.09 cm^2), the counter electrode was a platinum wire (Kurt J. Lesker, Jefferson Hills, PA; 99.99%, 0.5 mm diameter), and a silver wire immersed in electrolyte served as a quasireference electrode (CH Instruments). The reference was separated from the working solution by a Vycor frit (Bioanalytical Systems, Inc.). Ferrocene (Sigma Aldrich; twice-sublimed) was added to the electrolyte solution at the conclusion of each experiment (~1 mM); the midpoint potential of the ferrocenium/ferrocene couple (denoted as $Fc^{+/0}$) served as an external standard for comparison of the recorded potentials.

5.4. X-ray Crystallography

Crystals were mounted using Paratone oil with MiTeGen loops and placed under a nitrogen stream for data collection. Low-temperature (100 K) X-ray[please check and confirm] data were collected using 1°-wide ω- or φ-scans on a Bruker D8 Venture diffractometer with a Photon III CPAD detector equipped with Helios high-brilliance multilayer mirror optics. X-rays were provided by a IμS 3.0 Microfocus Mo sealed tube running at 50 kV and 1.4 mA (Mo Kα = 0.71 073 Å). All diffractometer manipulations, including data collection, integration, and scaling, were carried out using the Bruker APEX4 Software Suite.[63,64] All data manipulations were carried out using the Bruker APEX4 Software Suite and were corrected for absorption using the multi-scan method by SADABS.[65] SHELXT was used to solve each structure using intrinsic phasing methods.[66] Final stages of weighted full-matrix least-squares refinement were conducted using F_o^2 data with SHELXL in SHELXle.[67] Deposition Numbers 2 408 162 ([Ce] (e05a)), 2 408 163 ([Ce,Na] (e14a)), and 2 408 164 ([Ce,Ca] (e29a)) contain the supplementary crystallographic data for this paper. These data are provided free of charge by the joint Cambridge Crystallographic Data Centre and Fachinformationszentrum Karlsruhe Access Structures service.

The final structural model for each compound incorporated anisotropic thermal parameters for all nonhydrogen atoms; isotropic thermal parameters were used for all included hydrogen atoms. Hydrogen atoms associated with the ligand backbone in each complex were fixed at idealized riding model sp^2- or sp^3-hybridized positions with C—H bond lengths of 0.95–0.99 Å. Methyl groups were incorporated into the structural models either as sp^3-hybridized riding model groups with idealized "staggered" geometry and a C—H bond length of 0.98 Å or as idealized riding model rigid rotors (with a C—H bond length of 0.98 Å) that were allowed to rotate freely about their C—C bonds in least-squares refinement cycles. The isotropic thermal parameters of idealized hydrogen atoms in all three structures were fixed at values 1.2 (nonmethyl) or 1.5 (methyl) times the equivalent isotropic thermal parameter of the carbon or oxygen atom to which they are covalently bonded. With respect to the procedure applied to hydrogen atoms on outer-sphere water molecules, an initial check was done for Q peaks with reasonable positions and magnitudes. If found, hydrogen atoms were placed there and fixed. When the hydrogen atoms were not found in the difference map, their positions were refined with idealized positions and fixed. See the Special Refinement Details for each structure in the Supporting Information for more information.

5.5. Synthetic Procedures

5.5.1. Preparation of 3-(benzyloxy)-2-hydroxybenzaldehyde

The title compound was prepared according to literature procedures with minor modifications.[46] To a suspension of NaH (1.44 g, 0.055 mol) in dry tetrahydrofuran (50 mL) at 0 °C was added a solution of 2,3-dihydroxybenzaldehyde (3.03 g, 0.022 mol) in THF dropwise. The solution was allowed to warm to room temperature and stirred for 1 hour. Benzyl bromide (2.6 mL, 0.022 mol) was then added in a dropwise fashion, and the reaction mixture was heated at 60 °C for 48 hours. (The literature procedure on which the synthesis was based allowed the reaction to stir at 20 °C for 48 hours.[46]) The reaction mixture was then washed with water, and the aqueous layer was acidified to pH = 2 using 6 M HCl. Upon extraction with chloroform and drying, the volatiles were removed in vacuo, and the crude mixture was washed with diethyl ether over a silica plug. Recrystallization in ethanol yielded the title compound in a 27% yield (1.38 g). ^1H NMR (400z MHz, CD_3CN) δ 10.75 (s, 1H), 9.97 (s, 1H), 7.50–7.26 (m, 7H), 6.97 (t, J=7.9 Hz, 1H), 5.16 (s, 2H). ATR-IR: 3050–2877 (hydrogen-bonded OH stretching), 1650 (C=O stretching), 1640 (aromatic C=C stretching), 1450 (methylene C—H bending), 1380 (aldehyde C—H bending), 1240 (ether C—O bending), 760 and 690 (C—H bending of a 1,2,3-trisubstituted aromatic ring), 730 and 694 cm^{-1}

(C—H bending of monosubstituted aromatic rings). Both NMR and IR spectra agreed with previously reported characterization data.[46]

5.5.2. Preparation of H_3L^{OBn}

To a solution of 3-(benzyloxy)-2-hydroxybenzaldehyde (0.46 g, 2.0 mmol) in dry dichloromethane with molecular sieves was added tris(2-aminoethyl)amine (0.01 mL, 6.8 mmol) in a dropwise fashion under a slight flow of nitrogen. The reaction mixture was allowed to stir for 2 hours, after which the molecular sieves were removed via filtration. The title compound was obtained following the removal of volatiles in vacuo as a brownish-yellow solid (3.99 g, 99%). ^{1}H NMR (400 MHz, CD_3CN) δ 14.05 (s, 3H), 7.98 (s, 3H), 7.57–7.13 (m, 15H), 6.96 (dd, J = 8.0, 1.5 Hz, 3H), 6.50 (t, J = 7.9 Hz, 3H), 6.18 (dd, J = 7.8, 1.5 Hz, 3H), 5.09 (s, 6H), 3.54 (t, J = 5.5 Hz, 6H), 2.83 (t, J = 5.5 Hz, 6H). $^{13}C\{^1H\}$ NMR (100 MHz, CD_3CN) δ 167.32 (s), 153.84 (s), 148.18 (s), 138.56 (s), 129.42 (s), 128.83 (s), 128.76 (s), 125.12 (s), 119.77 (s), 118.41 (s), 117.89 (s), 71.70 (s), 58.19 (s), 56.31 (s). ATR-IR: 3050–2877 (hydrogen-bonded OH stretching), 1628 (imine C=N stretching), 1453 (methylene C—H bending), 1242 (ether C—O bending), 1063 (amine C—N stretching), 730 and 650 cm^{-1} (C—H bending of monosubstituted aromatic rings). ESI-MS (positive) m/z: 799.3477 (99%) ($H_3L^{OBn} + Na^+$), 800.3545 (54%), 801.3583 (15%).

5.5.3. Preparation of [Ce]

To a solution of H_3L^{OBn} (0.13 g, 0.21 mmol) in tetrahydrofuran was added $Ce(N(SiMe_3)_2)_3$ (0.16 g, 0.21 mmol) under an inert atmosphere, and the reaction mixture was stirred for 1 hour. The resulting mixture was filtered to yield the title compound as a metallic orange solid (0.15 g, 75%). Single orange crystals suitable for XRD analysis were obtained by vapor diffusion of Et_2O into a dilute solution of the title compound in CH_3CN. ^{1}H NMR (400 MHz, CD_2Cl_2) δ 17.57 (s, 3H), 10.66 (s, 3H), 8.12 (d, J = 7.3 Hz, 3H), 7.88 (t, J = 7.5 Hz, 3H), 6.52 (t, J = 7.3 Hz, 3H) 6.27 (s, J = 7.2 Hz, 6H), 4.86 (d, J = 7.6 Hz, 6H), 2.99 (s, 1H), 1.78 (s, 6H), 1.26 (s, 6H), -8.16 (s, 6H) ppm. $^{13}C\{^1H\}$ NMR (100 MHz, CD_2Cl_2) δ 136.61 (s), 131.07 (s), 128.25 (s), 127.69 (s), 126.01 (s), 125.82 (s), 122.24 (s), 117.60 (s), 69.68 (s) ppm. ATR-IR: 3050–2877 (hydrogen-bonded OH stretching), 1618 (imine C = N stretching), 1438 (methylene C—H bending), 1238 (ether C—O bending), 967 (amine C—N stretching), 730 and 650 cm^{-1} (C—H bending of monosubstituted aromatic rings). Anal. Calcd. for $C_{48}H_{45}N_4O_6Ce$ **[Ce]**: C 63.08, H 4.96, N 6.13; Found: C 60.31, H 4.68, N 5.62. Calc for $CeN_4O_6C_{48}H_{45} + 0.6(CH_2Cl_2)$: C 60.49, H 4.83, N 5.81. Dichloromethane inclusion in the sample was derived from crystallization conditions used to prepare bulk quantities of **[Ce]** for elemental analysis.

5.5.4. Preparation of [Ce,M]

To a suspension of **[Ce]** (1 equiv.) in minimal CH_3CN was added the corresponding metal salt ($M^{n+}(OTf)_n$) (0.95 equiv.) in minimal CH_3CN. The color of the reaction mixture rapidly lightened and became virtually fully homogeneous. The solution was filtered to remove any solid impurities, and volatiles were removed in vacuo to yield the desired **[Ce,M]** complexes.

[Ce,Na]: This complex was synthesized according to the above procedure in an 82% yield (0.097 g). Light orange single crystals suitable for XRD were obtained by vapor diffusion of Et_2O into CH_3CN. ^{1}H NMR (500 MHz, CD_3CN) δ 11.42 (s, 3H), 9.38 (s, 6H), 8.14 (s, 6H), 7.97 (s, 6H), 7.65 (d, J = 9.2 Hz, 3H), 7.30 (t, J = 7.4 Hz, 3H), 7.18 (t, J = 7.6 Hz, 6H), 6.68 (s, 6H), 5.98 (s, 6H) ppm. $^{13}C\{^1H\}$ NMR (126 MHz, CD_2Cl_2) δ 159.09 (s), 158.43 (s), 139.56 (s), 129.87 (s), 128.92 (s), 128.50 (s), 125.49 (s), 115.88 (s), 114.36 (s), 72.64 (s) ppm. ^{19}F NMR (470 MHz, CD_3CN) δ 80.26 (s) ppm. ATR-IR: 3145–2725 (hydrogen-bonded OH stretching), 1613 (imine C=N stretching), 1453 (methylene C—H bending), 1212 (ether C—O bending), 1037 (amine C—N stretching), 735 and 638 cm^{-1} (C—H bending of monosubstituted aromatic rings). Anal. Calcd. for $C_{49}H_{45}N_4O_9F_3SCeNa$ **[Ce,Na]**: C 54.19, H 4.18, N 5.16; Found: C 53.83, H 4.03, N 4.90.

[Ce,Ca]: This c was synthesized according to the above procedure in a 93% yield (0.132 g). Yellow single crystals suitable for XRD were obtained by vapor diffusion of pentane into a solution of the title compound in tetrahydrofuran. ^{1}H NMR (500 MHz, CD_3CN) δ 13.97 (s, 3H), 8.06 (s, 6H), 7.08 (d, J = 7.9 Hz, 3H), 6.99 (d, J = 7.9 Hz, 3H), 6.95 (m, 3H), 6.82 (t, J = 7.7 Hz, 6H), 6.69 (d, J = 7.8 Hz, 6H), 6.20 (t, J = 7.9 Hz, 3H), 5.74 (s, 6H), 3.74 (s, 6H) ppm. $^{13}C\{^1H\}$ NMR (126 MHz, CD_2Cl_2) δ 155.39 (s), 137.21 (s), 129.15 (s), 128.23 (s), 127.96 (s), 126.46 (s), 116.52 (s), 115.97 (s), 71.40 (s), 58.93 (s) ppm. ^{19}F NMR (470 MHz, CD_3CN) δ 80.17 (s) ppm. ATR-IR: 3115–2820 (hydrogen-bonded OH stretching), 1620 (imine C = N stretching), 1457 (methylene C—H bending), 1212 (ether C—O bending), 1031 (amine C—N stretching), 740 and 637 cm^{-1} (C—H bending of monosubstituted aromatic rings). Anal. Calcd. for $C_{50}H_{45}N_4O_{12}F_6S_2CeCa$ **[Ce,Ca]**: C 47.96, H 3.62, N 4.47; Found: C 47.96, H 3.76, N 4.35.

Supporting Information

The authors have cited additional references within the Supporting Information. The following files are available free of charge: NMR spectra, characterization data for the complexes reported here, and detailed information regarding the single-crystal X-ray diffraction analysis (PDF) Cartesian coordinates fors the structures from XRD (CIF, XYZ)

Acknowledgments

The authors thank Dr. Victor W. Day for helpful discussions and technical assistance with the structural data reported in this manuscript, Dr. William Brennesel (CENTC Elemental Analysis Facility, University of Rochester funded by NSF CHE-0650456), and Grant Arehart for assistance with collection of infrared spectra. This work was supported by the U.S. Department of Energy, Office of Science, Office of Basic Energy Sciences through the Early Career Research Program (DE-SC0019169). E.R.M. was supported by a U.S. National Science Foundation Research Traineeship (NRT) at the University of Kansas (DGE-1922649).

Conflict of Interests

The authors declare no conflict of interest.

Data Availability Statement

The data that support the findings of this study are available in the supplementary material of this article.

Keywords: electrochemistry · Lewis acids · redox chemistry · spectroscopy · X-ray diffraction

[1] P. B. Hitchcock, M. F. Lappert, L. Maron, A. V. Protchenko, *Angew. Chem. Int. Ed.* **2008**, *47*, 1488–1491.
[2] a) M. R. MacDonald, J. W. Ziller, W. J. Evans, *J. Am. Chem. Soc.* **2011**, *133*, 15914; b) M. R. MacDonald, J. E. Bates, M. E. Fieser, J. W. Ziller, F. Furche, W. J. Evans, *J. Am. Chem. Soc.* **2012**, *134*, 8420; c) M. R. MacDonald, J. E. Bates, J. W. Ziller, F. Furche, W. J. Evans, *J. Am. Chem. Soc.* **2013**, *135*, 9857; d) M. Xémard, A. Jaoul, M. Cordier, F. Molton, O. Cador, B. Le Guennic, C. Duboc, O. Maury, C. Clavaguéra, G. Nocton, *Angew. Chem. Int. Ed.* **2017**, *129*, 4330; e) M. Xémard, M. Cordlier, F. Molton, C. Duboc, B. Le Guennic, O. Maury, O. Cador, G. Nocton, *Inorg. Chem.* **2019**, *58*, 2872.
[3] a) N. T. Rice, I. A. Popov, D. R. Russo, J. Bacsa, E. R. Batista, P. Yang, J. Telser, H. S. La Pierre, *J. Am. Chem. Soc.* **2019**, *141*, 13222; b) T. P. Gompa, A. Ramanathan, N. T. Rice, H. S. La Pierre, *Dalton Trans.* **2020**, *49*, 15945; c) N. T. Rice, I. A. Popov, D. R. Russo, T. P. Gompa, A. Ramanathan, J. Bacsa, E. R. Batista, P. Yang, H. S. La Pierre, *Chem. Sci.* **2020**, *11*, 6149; d) T. P. Gompa, S. M. Greer, N. T. Rice, N. Jiang, J. Telser, A. Ozarowski, B. W. Stein, H. S. La Pierre, *Inorg. Chem.* **2021**, *60*, 9064; e) N. T. Rice, I. A. Popov, R. K. Carlson, S. M. Greer, A. C. Boggiano, B. W. Stein, J. Bacsa, E. R. Batista, P. Yang, H. S. La Pierre, *Dalton Trans.* **2022**, *51*, 6696; f) A. C. Boggiano, S. R. Chowdhury, M. D. Roy, M. G. Bernbeck, S. M. Greer, B. Vlaisavljevich, H. S. La Pierre, *Angew. Chem. Int. Ed.* **2024**, *63*, e202409789.
[4] a) C. T. Palumbo, I. Zivkovic, R. Scopelliti, M. Mazzanti, *J. Am. Chem. Soc.* **2019**, *141*, 9827; b) A. R. Willauer, C. T. Palumbo, R. Scopelliti, I. Zivkovic, I. Douair, L. Maron, M. Mazzanti, *Angew. Chem. Int. Ed.* **2020**, *59*, 3549; c) A. R. Willauer, C. T. Palumbo, F. Fadaei-Tirani, I. Zivkovic, I. Douair, L. Maron, M. Mazzanti, *J. Am. Chem. Soc.* **2020**, *142*, 5538; d) A. R. Willauer, I. Douair, A.-S. Chauvin, F. Fadaei-Tirani, J.-C. G. Bünzli, L. Maron, M. Mazzanti, *Chem. Sci.* **2022**, *13*, 681; e) M. Tricoire, F.-C. Hsueh, M. Keener, T. Rajeshkumar, R. Scopelliti, I. Zivkovic, L. Maron, M. Mazzanti, *Chem. Sci.* **2024**, *15*, 6874.
[5] T. Xue, Y.-S. Ding, X.-L. Jiang, L. Tao, J. Li, Z. Zheng, *Precis. Chem.* **2023**, *1*, 583.
[6] T. Xue, Y.-S. Ding, Z. Zheng, *Dalton Trans.* **2024**, *53*, 5779.
[7] a) G. A. Molander, *Chem. Rev.* **1992**, *92*, 29; b) A. Trovarelli, *Cat. Rev.* **1996**, *38*, 439; c) T. Bunluesin, R. J. Gorte, G. W. Graham, *Appl. Catal. B* **1998**, *15*, 107; d) E. P. Murray, T. Tsai, S. A. Barnett, *Nature* **1999**, *400*, 649; e) A. K. Das, *Coord. Chem. Rev.* **2001**, *213*, 307; f) Q. Fu, H. Saltsburg, M. Flytzani-Stephanopoulos, *Science* **2003**, *301*, 935; g) S. Kanai, I. Nagahara, Y. Kita, K. Kamata, M. A. Hara, *Chem. Sci.* **2017**, *8*, 3146; j) H. Tsurugi, K. Mashima, *J. Am. Chem. Soc.* **2021**, *143*, 7879.
[8] a) M. Suta, C. Wickleder, *J. Lumin.* **2019**, *210*, 210; b) G. Bousrez, F. Jaroschik, *Eur. J. Org. Chem.* **2022**, e202200202.
[9] N. A. Piro, J. R. Robison, P. J. Walsh, E. J. Schelter, *Coord. Chem. Rev.* **2014**, *360*, 21–36.
[10] D. F. Ghanotakis, G. T. Babcock, C. F. Yocum, *FEBS Lett.* **1984**, *167*, 127.
[11] a) E. Y. Tsui, J. S. Kanady, T. Agapie, *Inorg. Chem.* **2013**, *52*, 13833; b) E. Y. Tsui, T. Agapie, *Proc. Natl. Acad. Sci. USA* **2013**, *110*, 10084; c) P.-H. Lin, M. K. Takase, T. Agapie, *Inorg. Chem.* **2015**, *54*, 59.
[12] G. Wulfsberg, in *Principles of Descriptive Inorganic Chemistry*, University Science Books, **1991**, pp. 27–31.
[13] D. D. Perrin, in *Ionisation Constants of Inorganic Acids and Bases in Aqueous Solution*, 2nd ed., International Union of Pure and Applied Chemistry, Pergamon Press, Inc., **1982**.
[14] a) P. Erdmann, L. Greb, *ChemPhysChem* **2021**, *22*, 935; b) P. Erdmann, L. Greb, *Angew. Chem. Int. Ed.* **2022**, *134*, e202114550; c) P. Erdmann, M. Schmitt, L. M. Sigmund, F. Krämer, F. Breher, L. Greb, *Angew. Chem. Int. Ed.* **2024**, *63*, e202403356.
[15] a) A. Kumar, J. D. Blakemore, *Inorg. Chem.* **2021**, *60*, 1107; b) R. R. Golwankar, T. D. Curry II, C. J. Paranjothi, J. D. Blakemore, *Inorg. Chem.* **2023**, *62*, 9765.
[16] a) J. S. Kanady, E. Y. Tsui, M. W. Day, T. Agapie, *Science* **2011**, *333*, 733; b) Y. J. Park, S. A. Cook, N. S. Sickerman, Y. Sano, J. W. Ziller, A. S. Borovik, *Chem. Sci.* **2013**, *4*, 717; c) Y. Tsui, R. Tran, J. Yano, T. Agapie, *Nat. Chem.* **2013**, *5*, 293; d) A. H. Reath, J. W. Ziller, C. Tsay, A. J. Ryan, J. Y. Yang, *Inorg. Chem.* **2017**, *56*, 3713; e) T. Chantarojsiri, J. W. Ziller, J. Y. Yang, *Chem. Sci.* **2018**, *9*, 2567; f) D. Lionetti, S. Suseno, E. Y. Tsui, L. Lu, T. A. Stich, K. M. Carsch, R. J. Nielsen, W. A. Goddard III, R. D. Britt, T. Agapie, *Inorg. Chem.* **2019**, *58*, 2336; g) S. Maity, S. Ghosh, A. Ghosh, *Dalton Trans.* **2019**, *48*, 14898; h) A. C. Deacy, E. Moreby, A. Phanopoulos, C. K. Williams, *J. Am. Chem. Soc.* **2020**, *142*, 19150; i) N. G. Léonard, T. Chantarojsiri, J. W. Ziller, J. Y. Yang, *J. Am. Chem. Soc.* **2022**, *144*, 1503; j) T. K. Ghosh, S. Maity, S. Ghosh, R. M. Gomila, A. Frontera, A. Ghosh, *Inorg. Chem.* **2022**, *61*, 7130; k) H. M. Nguyen, H. W. T. Morgan, T. Chantarojsiri, T. A. Kerr, J. Y. Yang, A. N. Alexandrova, N. G. Léonard, *J. Phys. Chem. A* **2023**, *127*, 5324.
[17] A. Kumar, D. Lionetti, V. W. Day, J. D. Blakemore, *Chem. Eur. J.* **2017**, *24*, 141.
[18] A. Kumar, D. Lionetti, V. W. Day, J. D. Blakemore, *J. Am. Chem. Soc.* **2020**, *142*, 3032.
[19] A. Kumar, R. R. Golwankar, M. M. Pyrch, F. L. Cooper; G. A. Arehart; K. P. Carter, A. G. Oliver, V. W. Day, T. Z. Forbes, J. D. Blakemore, *Dalton Trans.* **2025**, https://doi.org/10.1039/D4DT03503H.
[20] S. R. Kelsey, A. Kumar, A. G. Oliver, V. W. Day, J. D. Blakemore, *ChemElectroChem* **2021**, *8*, 2792.
[21] a) J. P. Karnes, A. Kumar, J. A. Hopkins Leseberg, V. W. Day, J. D. Blakemore, *Inorg. Chem.* **2024**, *63*, 8710; b) J. P. Karnes, A. G. Oliver, C. S. Day, V. W. Day, J. D. Blakemore, *Inorg. Chem.* **2025**, *64*, 571.
[22] R. R. Golwankar, A. Kumar, V. W. Day, J. D. Blakemore, *Chem. Eur. J.* **2022**, *28*, e202200344.
[23] C. M. Dopp, R. R. Golwankar, S. R. Kelsey, J. T. Douglas, A. N. Erickson, A. G. Oliver, V. W. Day, C. S. Day, J. D. Blakemore, *Inorg. Chem.* **2023**, *62*, 9827.
[24] G. B. Panetti, J. R. Robinson, E. J. Schelter, P. J. Walsh, *Acc. Chem. Res.* **2021**, *54*, 2637.
[25] J.-C. G. Bünzli, C. Piguet, *Chem. Rev.* **2002**, *102*, 1897.
[26] J. R. Robinson, Z. Gordon, C. H. Booth, P. J. Carroll, P. J. Walsh, E. J. Schelter, *J. Am. Chem. Soc.* **2013**, *135*, 19016.
[27] S. Liu, L. W. Yang, S. J. Rettig, C. Orvig, *Inorg. Chem.* **1993**, *32*, 2773.
[28] J.-P. Costes, F. Dahan, A. Dupuis, S. Lagrave, J.-P. Laurent, *Inorg. Chem.* **1998**, *37*, 153.
[29] A. C. Boggiano, C. M. Studvick, A. Steiner, J. Basta, I. A. Popov, H. S. La Pierre, *Chem. Sci.* **2023**, *14*, 11708.
[30] J. A. Leseberg, T. P. Gompa, E. R. Mikeska, A. G. Oliver, V. W. Day, H. S. La Pierre, J. D. Blakemore, *ChemRxiv preprint* **2025**, https://doi.org/10.26434/chemrxiv-2024-sbzfx-v2.
[31] J. L. Hoard, H. H. Nordsieck, *J. Am. Chem. Soc.* **1939**, *61*, 2853.
[32] J. L. Hoard, J. V. Silverton, *Inorg. Chem.* **1963**, *2*, 235.
[33] J. V. Silverton, J. L. Hoard, *Inorg. Chem.* **1963**, *2*, 243.
[34] V. W. Day, J. L. Hoard, *J. Am. Chem. Soc.* **1970**, *92*, 3626.
[35] E. L. Muetterties, C. M. Wright, *Q. Rev. Chem. Soc.* **1967**, *21*, 109.
[36] A. Smith, S. J. Rettig, C. Orvig, *Inorg. Chem.* **1988**, *27*, 3929.
[37] D. J. Berg, S. J. Rettig, C. Orvig, *J. Am. Chem. Soc.* **1991**, *113*, 2528.
[38] S. Liu, L. Gelmini, S. J. Rettig, R. C. Thompson, C. Orvig, *J. Am. Chem. Soc.* **1992**, *114*, 6081.
[39] S. J. Archibald, A. J. Blake, S. Parsons, M. Schröder, R. E. P. Winpenny, *J. Chem. Soc. Dalton Trans.* **1997**, *2*, 173.
[40] J.-P. Costes, F. Dahan, F. Nicodème, *Inorg. Chem.* **2003**, *42*, 6556.
[41] P. Bag, A. Chakraborty, M. Rouzières, R. Clérac, R. J. Butcher, V. Chandrasekhar, *Cryst. Growth Des.* **2014**, *14*, 4583.
[42] E. Lucaccini, J. J. Baldoví, L. Chelazzi, A.-B. Barra, F. Grepioni, J.-P. Costes, L. Sorace, *Inorg. Chem.* **2017**, *56*, 4728.
[43] A. Costache, A. M. Mădălan, *Rev. Roum. Chim.* **2020**, *65*, 761.
[44] J.-P. Costes, C. Duhayon, L. Vendier, W. Wernsdorfer, *Polyhedron* **2023**, *246*, 116699.
[45] a) M. Kanesato, M. Goto, CCDC 801630: Experimental Crystal Structure Determination, **2017**, https://doi.org/10.5517/ccdc.csd.ccvx52z; b) M. Kanesato, M. Goto, CCDC 801631: Experimental Crystal Structure Determination, **2017**, https://doi.org/10.5517/ccdc.csd.ccvx51y.
[46] K. A. Parker, A. T. Georges, *Org. Lett.* **2000**, *2*, 497.
[47] E. J. Corey, J. C. Bailar Jr., *J. Am. Chem. Soc.* **1959**, *81*, 2620.
[48] R. D. Shannon, *Acta Cryst. A.* **1976**, *32*, 751.
[49] M. Y. Livshits, N. J. Wolford, J. K. Banh, M. M. MacInnes, S. M. Greer, J. S. R. V. Winfred, K. Hanson, T. P. Gompa, B. W. Stein, *Inorg. Chem.* **2023**, *62*, 13712.
[50] X.-L. Zheng, Y. Liu, M. Pan, X.-Q. Lü, Y.-Y. Zhang, C.-Y. Zhao, Y.-X. Tong, C.-Y. Su, *Angew. Chem. Int. Ed.* **2007**, *46*, 7399.

[51] H. Yin, P. J. Carroll, J. M. Anna, E. J. Schelter, *J. Am. Chem. Soc.* **2015**, *137*, 9234.
[52] V. A. Ilichev, L. I. Silantyeva, I. D. Grishin, A. V. Rozkhov, R. V. Rumyantcev, G. K. Fukin, M. N. Bochkarev, *RSC Adv.* **2019**, *9*, 24110.
[53] P. Thordarson, *Chem. Soc. Rev.* **2011**, *40*, 1305.
[54] a) A. V. Hill, *J. Physiol.* **1910**, *40*, 4; b) I. Langmuir, *J. Am. Chem. Soc.* **1918**, *40*, 1361; c) J. M. Berg, J. L. Tymoczko, L. Stryer, in *Biochemistry*, Macmillin, **2007**, pp. 210–211.
[55] Y. Morimoto, H. Kotani, J. Park, Y.-M. Lee, W. Nam, S. Fukuzumi, *J. Am. Chem. Soc.* **2011**, *133*, 403.
[56] H. Yoon, Y.-M. Lee, X. Wu, K.-B. Cho, R. Sarangi, W. Nam, S. Fukuzumi, *J. Am. Chem. Soc.* **2013**, *135*, 9186.
[57] M. Sankaralingam, Y.-M. Lee, Y. Pineda-Galvan, D. G. Karmalkar, M. S. Seo, S. H. Jeon, Y. Pushkar, S. Fukuzumi, *J. Am. Chem. Soc.* **2019**, *141*, 1324.
[58] D. Lionetti, S. Suseno, A. A. Shiau, G. de Ruiter, T. Agapie, *JACS Au* **2024**, *4*, 344.
[59] D. C. Bradley, J. S. Ghotra, F. A. Hart, *J. Chem. Soc. Dalton Trans.* **1973**, 1021.
[60] G. R. Fulmer, A. J. M. Miller, N. H. Sherden, H. E. Gottlieb, A. Nudelman, B. M. Stoltz, J. E. Bercaw, K. I. Goldberg, *Organometallics* **2010**, *29*, 2176.
[61] R. K. Harris, E. D. Becker, S. M. C. de Menezes, R. Goodfellow, P. Granger, *Pure Appl. Chem.* **2001**, *73*, 1795.
[62] R. K. Harris, E. D. Becker, S. M. C. de Menezes, P. Granger, R. E. Hoffman, K. W. Zilm, *Pure Appl. Chem.* **2008**, *80*, 59.
[63] APEX-4, Bruker Analytical X-ray Systems Inc., Madison, WI USA **2022**.
[64] *SAINT Ver. 8.40A. Bruker Analytical X-ray Systems Inc.*, Madison, WI USA **2022**.
[65] G. M. Sheldrick, in *SADABS (version 2008/1): Program for Absorption Correction for Data from Area Detector Frames*, University of Göttingen, **2008**.
[66] a) G. M. Sheldrick, *Acta Crystallogr., Sect. A: Found. Crystallogr.* **2015**, *71*, 3; b) G. M. Sheldrick, CELL_NOW, Georg-August-Universität, Göttingen, Germany **2008**.
[67] C. B. Hübschle, G. M. Sheldrick, B. Dittrich, *J. Appl. Cryst.* **2011**, *44*, 1281.

Manuscript received: February 6, 2025
Revised manuscript received: April 15, 2025
Version of record online: May 6, 2025